

---

# Testing Robustness Against Unforeseen Adversaries

---

**Daniel Kang\***  
Stanford University  
ddkang@stanford.edu

**Yi Sun\***  
Columbia University  
yisun@math.columbia.edu

**Dan Hendrycks**  
UC Berkeley  
hendrycks@berkeley.edu

**Tom Brown**  
OpenAI  
tom@openai.com

**Jacob Steinhardt**  
OpenAI, UC Berkeley  
jsteinhardt@berkeley.edu

## Abstract

Considerable work on adversarial defense has studied robustness to a fixed, known family of adversarial distortions, most frequently  $L_p$ -bounded distortions. In reality, the specific form of attack will rarely be known and adversaries are free to employ distortions outside of any fixed set. The present work advocates measuring robustness against this much broader range of *unforeseen attacks*—attacks whose precise form is not known when designing a defense.

We propose a methodology for evaluating a defense against a diverse range of distortion types together with a summary metric UAR that measures the Unforeseen Attack Robustness against a distortion. We construct novel JPEG, Fog, Gabor, and Snow adversarial attacks to simulate unforeseen adversaries and perform a careful study of adversarial robustness against these and existing distortion types. We find that evaluation against existing  $L_p$  attacks yields highly correlated information that may not generalize to other attacks and identify a set of 4 attacks that yields more diverse information. We further find that adversarial training against either one or multiple distortions, including our novel ones, does not confer robustness to unforeseen distortions. These results underscore the need to study robustness against unforeseen distortions and provide a starting point for doing so.

## 1 Introduction

Neural networks perform well on many benchmark tasks [1] yet can be fooled by adversarial examples [2], slightly distorted inputs designed to subvert a given model. The adversary is frequently assumed to craft adversarial distortions under an  $L_\infty$  constraint [2, 3, 4], while other distortions such as adversarial geometric transformations, patches, and even 3D-printed objects [5, 6, 7] have also been considered. However, most work on adversarial robustness assumes the adversary is *fixed* and known. Defenses against adversarial attacks often leverage such knowledge when designing the defense, most commonly through adversarial training [3], which minimizes the adversarial loss against a fixed distortion type.

In practice, adversaries can modify their attacks and can construct distortions whose precise form is not known to the defense designers. The present work proposes a methodology for assessing robustness to such *unforeseen attacks* and uses it to study how adversarial robustness transfers to them. We propose evaluating defenses against a diverse set of unforeseen or held-out distortions that are decoupled from the defense’s design. For any given held-out distortion, we evaluate while controlling for the crucial variable of distortion size by considering an initially wide range of distortion sizes, measuring the corresponding attack strength using adversarial training for each distortion type, and conducting the final evaluation on a calibrated range of distortion sizes that is roughly comparable

---

\*Equal contribution

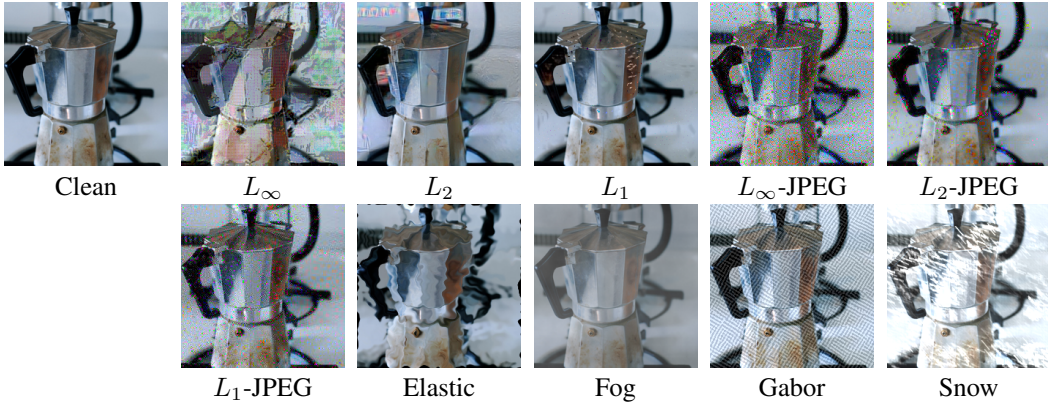


Figure 1: Attacked images (label “espresso maker”) against adversarially trained models with large  $\epsilon$ . Each of the adversarially attacked images above are optimized to maximize the classification loss.

across distortions. We collect this final evaluation in the summary metric UAR (Unforeseen Attack Robustness), which measures robustness of a defense against a distortion relative to the performance of a model adversarially trained on that distortion.

Using our proposed methodology, we provide a case study (Section 3) involving 87 different adversarially trained models against 87 attacks using the 10 distortions in Figure 1. For our case study, we develop four novel adversarial attacks: adversarial JPEG, Fog, Gabor, and Snow (Section 2). Code for evaluation and adversarial training, trained models, and results are available at <https://github.com/ddkang/advex-uar>.

Our case study reveals that numerous adversarial defenses do not provide robustness to unforeseen adversaries. We discover a strong negative result: adversarial training against a single distortion can *hurt* performance against other distortions. This applies even to the commonly used  $L_\infty$  defense; Figure 2 illustrates typical behavior where adversarial training helps at small  $\epsilon$  but hurts at larger  $\epsilon$ . Moreover, accuracy against different  $L_p$  distortions is highly correlated relative to the several other distortions we consider, suggesting that the common practice of evaluating only against  $L_p$  distortions can give a misleading account of a model’s adversarial robustness. These and many other observations from our full study (Section 4) add to the mounting evidence [8, 9, 10] that achieving robustness against a single distortion type is insufficient to impart robustness to unforeseen attacks.

A natural next approach is to defend against multiple distortion types simultaneously in the hope that this will cover a larger space of seen distortions and provide greater transfer to unforeseen distortions. Unfortunately, we find that hardening against even two different distortion types via joint adversarial training is difficult. Specifically, we identify a phenomenon whereby training against multiple distortions leads to overfitting at even moderate distortion sizes.

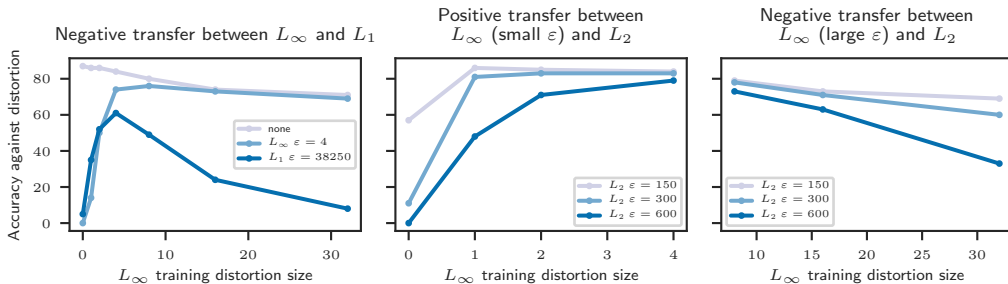


Figure 2: Accuracies of adversarially trained ResNet-50 models on ImageNet-100. **Left:** Training against  $L_\infty$  hurts robustness to  $L_1$ . **Middle, right:** Evaluating  $L_\infty$ -training on a restricted range of  $\epsilon$  gives misleading and opposite impressions about transfer to  $L_2$ .

Finally, we investigate the hypothesis recently suggested by Ford et al. [11] that adversarial examples arise from amplifying stochastic corruptions. We evaluate our adversarially trained models on the ImageNet-C benchmark [12], a recent dataset for corruption robustness consisting of ImageNet images with common visual corruptions instead of worst-case ones (Section 5). We find that adversarial robustness generally transfers to corruption robustness, but adversarial distortions and common corruptions of the same type can have opposite effects on models. We hypothesize that this effect arises from the drop in clean accuracy of adversarially trained models—common corruptions are easier than adversarial distortions, meaning the increased robustness of our models does not make up for the drop in clean accuracy.

## 2 Adversarial attacks

We consider distortions (attacks) applied to an image  $x \in \mathbb{R}^{3 \times 224 \times 224}$ , represented as a vector of RGB values. Let  $f : \mathbb{R}^{3 \times 224 \times 224} \rightarrow \mathbb{R}^{100}$  be a model mapping images to logits<sup>2</sup>, and let  $\ell(f(x), y)$  denote the cross-entropy loss. For an input  $x$  with true label  $y$  and a target class  $y' \neq y$ , our adversarial attacks attempt to find  $x'$  such that

1. the attacked image  $x'$  is obtained by applying a constrained distortion to  $x$ , and
2. the loss  $\ell(f(x'), y')$  is minimized (targeted attack).

Adversarial training [2] is a strong defense baseline against a fixed attack [3, 4] which updates using an attacked image  $x'$  instead of the clean image  $x$  at each training iteration.

We consider 10 attacks:  $L_\infty$  [2],  $L_2$  [13, 14],  $L_1$  [15], Elastic [16],  $L_\infty$ -JPEG,  $L_2$ -JPEG,  $L_1$ -JPEG, Fog, Gabor, and Snow. The JPEG, Fog, Gabor, and Snow attacks are new to this paper, and the  $L_1$  attack is a principled improvement on previous  $L_1$  attacks based on the Frank-Wolfe algorithm. We now describe the attacks, whose strengths are controlled by a size parameter  $\varepsilon$ ; sample images are in Figure 1. We clamp output pixel values to  $[0, 255]$ .

The  $L_p$  attacks with  $p \in \{1, 2, \infty\}$  modify an image  $x$  to an attacked image  $x' = x + \delta$ . We optimize  $x'$  under the constraint  $\|x' - x\|_p \leq \varepsilon$ , where  $\|\cdot\|_p$  denotes the  $L_p$ -norm on  $\mathbb{R}^{3 \times 224 \times 224}$ .

As discussed in [17] for defense, JPEG compression applies a lossy linear transformation based on the discrete cosine transform (denoted by JPEG) to image space, followed by quantization. The  $L_p$ -JPEG attacks for  $p \in \{1, 2, \infty\}$  impose the  $L_p$ -constraint  $\|\text{JPEG}(x) - \text{JPEG}(x')\|_p \leq \varepsilon$  on the attacked image  $x'$ . We optimize  $z = \text{JPEG}(x')$  and apply a right inverse of JPEG to obtain  $x'$ .

The Elastic attack allows distortions  $x' = \text{Flow}(x, V)$ , where  $V : \{1, \dots, 224\}^2 \rightarrow \mathbb{R}^2$  is a vector field on pixel space, and Flow sets the value of pixel  $(i, j)$  to the bilinearly interpolated original value at  $(i, j) + V(i, j)$ . We construct  $V$  by smoothing an initial vector field  $W$  by a Gaussian kernel (size  $25 \times 25$ , standard deviation 3 for a  $224 \times 224$  image), and optimize  $W$  under the constraint  $\|W(i, j)\|_\infty \leq \varepsilon$  for all  $i, j$ . Our attack differs in details from [16] but is similar in spirit.

Our novel Fog, Gabor, and Snow attacks are adversarial versions of non-adversarial distortions proposed in the literature. Stochastic versions of Fog and Snow appeared as common corruptions in [12], while the Gabor attack is based on additive Gabor noise [18, 19]. They each work by optimizing over a set of parameters controlling the distortion. For instance, adversarial fog is created in a way similar to the synthetic fog of [20]; however, the values used in the diamond-square algorithm to generate the fog are not uniformly sampled but adversarially determined through gradient descent. For Gabor, the sparse noise used to synthesize Gabor noise is found adversarially. Finally, for adversarial snow the brightness of each snowflake is adversarially optimized.

**Optimization.** To handle  $L_\infty$  and  $L_2$  constraints, we use randomly-initialized projected gradient descent (PGD), which optimizes the distortion  $\delta$  by gradient descent and projection to the  $L_\infty$  and  $L_2$  balls [3]. For  $L_1$  constraints, this projection is more difficult, and previous  $L_1$  attacks resort to heuristics [15, 10]. We instead use the randomly-initialized Frank-Wolfe algorithm [21], which consists of the following iterates for a constraint set  $\mathcal{C}$  (see Appendix B for pseudocode):

- Compute  $\nabla f(x_t)$  and  $s_t = \arg\min_{s \in \mathcal{C}} s^\top \nabla f(x_t)$ .
- Update  $x_{t+1} \leftarrow (1 - \eta_t)x_t + \eta_t s_t$  for step size  $\eta_t$ .

<sup>2</sup>We describe the attacks for ImageNet-100, but they can also be applied to CIFAR-10, which has 10 classes and  $32 \times 32$  images.

Frank-Wolfe only requires optimizing a linear function at each step, which is simpler than projecting. For the Elastic, Fog, Gabor, and Snow attacks, we similarly use PGD. Because the optimization problem for these attacks is difficult, we are not confident that PGD approximates the worst-case perturbation for these attacks, though it nevertheless yields a strong attack in most cases.

### 3 Methodology for assessing robustness against unforeseen adversaries

We now propose a method to assess robustness against unforeseen distortions, which relies on evaluating a defense against a diverse set of attacks that were *not* used when designing the defense. Our method must address the following issues:

- The range of distortion sizes considered must be wide enough to avoid the misleading behavior in the middle and right panels of Figure 2;
- The set of attacks considered must be sufficiently diverse.

We will first provide a method to calibrate distortion sizes and then use it to define a summary metric that assesses the robustness of a defense against a specific unforeseen attack. Using this metric, we are able to assess diversity and recommend a set of attacks to evaluate against.



(a) Many attacks, especially  $L_1$ -JPEG, appear small against undefended models but cause perceptually large distortions against defended models. The elastic attack is a notable exception to this effect. (b) The  $L_\infty$  attack at  $\epsilon = 32$  applied to an undefended model and to models adversarially trained against  $L_\infty$  at different distortion sizes. Attacking models trained against larger  $\epsilon$  produces greater visual distortion.

Figure 3: Defended models are needed to reveal full distortion strength.

**Calibrate distortion size using adversarial training.** As we saw in Figure 2, the correlation between adversarial robustness against different distortion types depends on the range of distortion sizes considered, meaning it is important to evaluate on wide enough ranges. We ideally want our largest distortion to yield barely recognizable images or to zero out the performance of all models. Figure 3 shows that attacking adversarially trained models (rather than regular models) is necessary to uncover the full strength of a distortion, and we therefore select our distortion sizes based on the following principles:

1. Models adversarially trained against the minimum distortion size should have adversarial accuracy on the validation set comparable to that of a model trained on unattacked data.
2. Attacks with the maximum distortion size should substantially reduce adversarial accuracy on the validation set in adversarial training or perturb the images enough to confuse humans.

This ensures that our distortion sizes range from being trivial to accommodate to being too strong either for a human or for an adversarially trained model.

**UAR: an adversarial robustness metric.** We measure a model’s robustness against a specific unforeseen distortion type by comparing it to adversarial training, which represents an approximate ceiling on performance with prior knowledge of the distortion type. For distortion type  $A$  and size  $\epsilon$ , let the Adversarial Training Accuracy  $ATA(A, \epsilon)$  be the best adversarial accuracy on the validation

Table 1: ATA values for different distortion types and sizes on ImageNet-100. ATA values for CIFAR-10 are shown in Table 3 (Appendix C.3.2).

Attack	$\varepsilon_1$	$\varepsilon_2$	$\varepsilon_3$	$\varepsilon_4$	$\varepsilon_5$	$\varepsilon_6$	ATA <sub>1</sub>	ATA <sub>2</sub>	ATA <sub>3</sub>	ATA <sub>4</sub>	ATA <sub>5</sub>	ATA <sub>6</sub>
$L_\infty$	1	2	4	8	16	32	84.6	82.1	76.2	66.9	40.1	12.9
$L_2$	150	300	600	1200	2400	4800	85.0	83.5	79.6	72.6	59.1	19.9
$L_1$	9562.5	19125	76500	153000	306000	612000	84.4	82.7	76.3	68.9	56.4	36.1
$L_\infty$ -JPEG	0.062	0.125	0.250	0.500	1	2	85.0	83.2	79.3	72.8	34.8	1.1
$L_2$ -JPEG	8	16	32	64	128	256	84.8	82.5	78.9	72.3	47.5	3.4
$L_1$ -JPEG	256	1024	4096	16384	65536	131072	84.8	81.8	76.2	67.1	46.4	41.8
Elastic	0.250	0.500	2	4	8	16	85.9	83.2	78.1	75.6	57.0	22.5
Fog	128	256	512	2048	4096	8192	85.8	83.8	79.0	68.4	67.9	64.7
Snow	0.062	0.125	0.250	2	4	8	84.0	81.1	77.7	65.6	59.5	41.2
Gabor	6.250	12.500	25	400	800	1600	84.0	79.8	79.8	66.2	44.7	14.6

set that can be achieved by adversarially training a specific architecture (ResNet-50 for ImageNet-100, ResNet-56 for CIFAR-10) against  $A$ .<sup>3</sup> Even when evaluating a defense using an architecture other than ResNet-50 or ResNet-56, we recommend using the fixed ATA values computed with these architectures to allow for uniform comparisons.

Given a set of distortion sizes  $\{\varepsilon_1, \dots, \varepsilon_n\}$ , we propose the summary metric UAR (*Unforeseen Attack Robustness*) normalizing the accuracy of a model  $M$  against adversarial training accuracy:

$$\text{UAR}(A, M) := 100 \cdot \left( \frac{1}{n} \sum_{k=1}^n \text{Acc}(A, \varepsilon_k, M) \right) / \left( \frac{1}{n} \sum_{k=1}^n \text{ATA}(A, \varepsilon_k) \right). \quad (1)$$

Here  $\text{Acc}(A, \varepsilon, M)$  is the accuracy of  $M$  against distortions of type  $A$  and magnitude  $\varepsilon$ . We expect most UAR scores to be lower than 100 against held-out distortion types, as an UAR score greater than 100 means that a defense is outperforming an adversarially trained model on that distortion.

Having too many or too few  $\varepsilon_k$  values in a certain range may cause an attack to appear artificially strong or weak because the functional relation between distortion size and attack strength (measured by ATA) varies between attacks. To compare attacks of different distortion types, we evaluate at  $\varepsilon$  increasing geometrically by factors of 2 and take the subset of  $\varepsilon$  whose ATA values have minimum  $\ell_1$ -distance to the ATA values of the  $L_\infty$  attack at geometrically increasing  $\varepsilon$ . We provide these numbers in Table 1 (Section 4) and use UAR in Section 4.2 to evaluate adversarially trained defenses.

**Evaluate against diverse distortion types.** Since increasing robustness against one distortion type can *decrease* robustness against others (Figure 2), measuring performance on different distortions is important to avoid overfitting to a specific type, especially when a defense is constructed with it in mind (as with adversarial training). Our case study in Section 4.2 reveals that choosing appropriate distortion types to evaluate against requires some care, as distortions such as  $L_p$  that may seem different can actually have highly correlated behavior (see Figure 4). We instead recommend evaluation against the  $L_1$ ,  $L_2$ -JPEG, Elastic, and Fog attacks as a starting point.

**Practical computational considerations.** For the 10 distortion types we consider, we provide reference values of  $\text{ATA}(A, \varepsilon)$  on a calibrated range of 6 distortion sizes on ImageNet-100 (Table 1) and CIFAR-10 (Table 3). This allows UAR evaluations for a new defense by performing 6 adversarial evaluations. A single evaluation on ImageNet-100 requires 1 GPU-hour on an NVIDIA V100, compared to 192+ GPU-hours for adversarial training, meaning this greatly reduces evaluation cost.

## 4 A case study on adversarial training using UAR

We conduct adversarial training and evaluation experiments on the attacks introduced in Section 2 to justify our methodology and provide calibrated ranges of distortion sizes on two datasets.

<sup>3</sup>As explained in Figure 10 (Appendix C.1), this usually requires training at distortion size  $\varepsilon' > \varepsilon$  because the typical distortion seen during adversarial training is sub-maximal.

## 4.1 Experimental setup

**Dataset and model.** We use two datasets: CIFAR-10 and ImageNet-100, the 100-class subset of ImageNet-1K [22] containing every 10th class by WordNet ID order. For CIFAR-10, we use the ResNet-56 [1] architecture. For ImageNet-100, we use the ResNet-50 [1] architecture with  $224 \times 224$  resolution as implemented in `torchvision`. We describe training hyperparameters in Appendix A.

**Adversarial training and evaluation procedure.** We construct hardened models using adversarial training [3]. To train against attack  $A$ , for each mini-batch of training images, we select a target class for each image uniformly at random from the set of incorrect classes. For a maximum distortion size  $\varepsilon$ , we generate adversarial images by applying the targeted attack  $A$  to the current model with distortion size  $\varepsilon' \sim \text{Uniform}(0, \varepsilon)$ ; this random scaling improves performance especially against smaller distortions. We update the model with a step of stochastic gradient descent using only the adversarial images (no clean images).

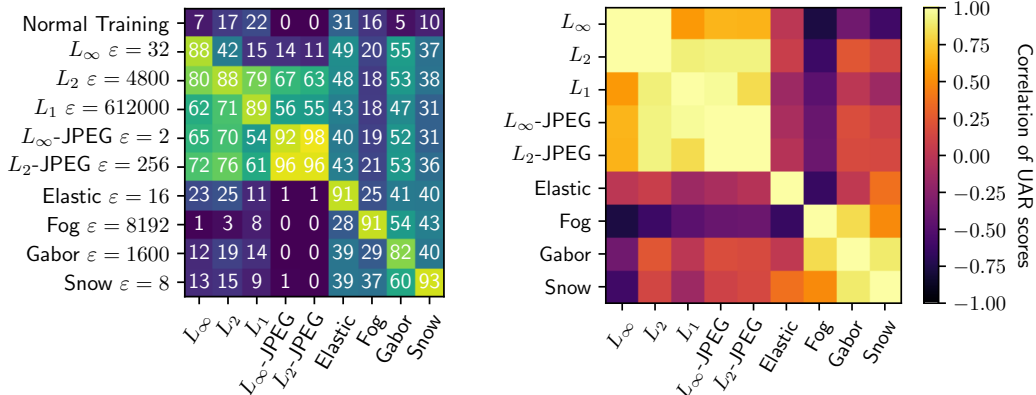
We use 10 optimization steps for all attacks during training except for Elastic, where we use 30 steps due to the greater difficulty of its optimization problem. When PGD is used, we choose step size  $\varepsilon/\sqrt{\text{steps}}$ , motivated by the optimal scaling for non-smooth convex functions [23, 24].

We evaluate on the ImageNet-100 and CIFAR-10 validation sets against 200-step targeted attacks with uniform random (incorrect) target class, using more steps for evaluation than training per best practices [25]. Figures 8 and 11 (Appendix C.1) present exhaustive adversarial training and evaluation results, which are summarized in Section 4.2 below. We perform robustness checks (to random seed and number of attack steps) in Appendix D.

**Choosing a calibrated range of distortion sizes.** Following Section 3, we trained against  $\varepsilon$  increasing geometrically from  $\varepsilon_{\min}$  to  $\varepsilon_{\max}$  by factors of 2. We choose  $\varepsilon_{\min}$  small enough so that a model adversarially trained against distortions of size  $\varepsilon_{\min}$  has adversarial accuracy close to the clean accuracy of an unattacked model. We choose  $\varepsilon_{\max}$  by increasing  $\varepsilon$  geometrically with ratio 2 until the adversarial accuracy of an adversarially trained model drops below 25 or the resulting images are not human-recognizable. Applying the calibration procedure of Section 3 yields the  $\varepsilon$  and ATA values in Table 1, which we suggest the community use to evaluate robustness to unforeseen adversaries.

## 4.2 Adversarial training against a single distortion type

We use UAR (Equation 1) to assess adversarial robustness against unforeseen attacks for adversarially trained models. Figure 4(a) displays UAR for models adversarially trained against each of the attacks



(a) UAR scores for adv. trained defenses (rows) against attack types (columns) on ImageNet-100. Additional values of  $\varepsilon$  are in Figure 9. CIFAR-10 results are in Appendix C.3.2. (b) Correlations between UAR scores in (a) for each attack type (rows and columns). Correlation was computed over adversarial defenses trained without knowledge of the attacks (7 total per attack pair).

Figure 4: UAR scores demonstrate the need to evaluate against diverse attacks.

on ImageNet-100 ( $L_1$ -JPEG omitted for space). We draw the following conclusions from trends in UAR and refer the interested reader to Appendix C.1 for complete evaluation statistics.

**Adversarial training against a fixed distortion is not robust to unforeseen attacks.** Figure 4(a) demonstrates that adversarially trained models against each of our fixed distortions have low UAR scores against several unforeseen distortions. For example, we were not able to achieve a high UAR against Fog except by directly adversarially training against it.

**Evaluating against  $L_p$  attacks can give highly correlated information.** Figure 4(b) reports correlation coefficients between UAR scores of pairs of attacks  $A$  and  $A'$ , with scores viewed as random vectors; we exclude defenses adversarially trained against  $A$  and  $A'$  to ensure that attacks are unforeseen. The correlations demonstrate that UAR scores of non- $L_p$  defenses against  $L_p$ -attacks are highly correlated, which suggests that evaluating on different  $L_p$  attacks offers little diversity. A similar correlation holds for the Fog, Gabor, and Snow attacks, which is not obvious given their disparate distortion types and illustrates that finding diverse distortions is a non-trivial task.

**Evaluate against  $L_1$ ,  $L_2$ -JPEG, Elastic, and Fog attacks as a starting point for diversity.** Figure 4(b) shows that UAR scores against the Elastic and Fog attacks have low correlation to scores against the  $L_p$ -attacks and each other, providing more diversity. We therefore propose the  $L_1$ ,  $L_2$ -JPEG, Elastic, and Fog attacks as a starting point for diverse evaluation.

### 4.3 Joint adversarial training

A natural idea for improving transfer is adversarially training the same model against two different types of distortions simultaneously, which we refer to as *joint adversarial training* [9, 10]. This procedure considers two attacks  $A$  and  $A'$ . At each training step, we compute the attacked image under both  $A$  and  $A'$  and backpropagate with respect to gradients induced by the image with greater loss. This corresponds to the “max” loss described in [10]. We jointly train models for  $(L_\infty, L_2)$ ,  $(L_\infty, L_1)$ , and  $(L_\infty, \text{Elastic})$  using the same setup as before.

**Transfer for jointly trained models.** Figure 5 reports UAR scores for jointly trained models using ResNet-50 on ImageNet-100; full evaluation accuracies are in Figure 17 (Appendix E). Comparing to the relevant rows of Figure 4(a) and Figure 9 (Appendix E), we see that, relative to  $L_2$  only, joint training against  $(L_\infty, L_2)$  slightly improves transfer against  $L_1$  without harming transfer against other attacks. In contrast, training against  $(L_\infty, L_1)$  is worse than *either* training against  $L_1$  or  $L_\infty$  separately (except at small  $\varepsilon$  for  $L_1$ ). Training against  $(L_\infty, \text{Elastic})$  also performs poorly.

**Joint training and overfitting.** What causes the poor performance of joint training? Jointly trained models achieve high *training* accuracy, but achieve poor validation accuracy (Table 2) that also fluctuates substantially across different random seeds. The joint training curve in Figure 6 illustrates the overfitting behavior for  $(L_\infty, \text{Elastic})$ : validation accuracy against the elastic attack decreases significantly while training accuracy continues to increase. This contrasts with the behavior we observe for regular adversarial training, where validation accuracy levels off as training accuracy increases.

Overfitting primarily occurs when training against large distortions. We successfully trained the  $(L_\infty, L_1)$  and  $(L_\infty, \text{Elastic})$  pairs for small distortion sizes, with accuracies comparable to but slightly lower than observed in Figure 8 for training against each attack individually. These results are given in Figure 16 (Appendix E), and agree with behavior reported by [10] on CIFAR-10. Our general intuition is that harder training tasks (more diverse distortion types, larger  $\varepsilon$ ) make overfitting more

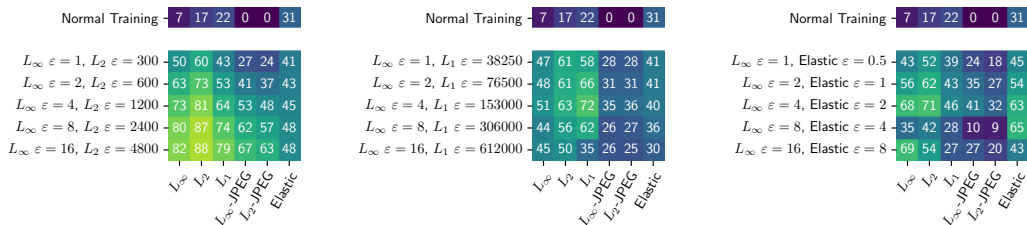


Figure 5: UAR scores for jointly adv. trained defenses (rows) against distortion types (columns).

Table 2: Train and val accuracies for joint adversarial training at large distortion are dependent on seed. For train and val,  $\varepsilon'$  is chosen uniformly at random between 0 and  $\varepsilon$ , and we used 10 steps for  $L_\infty$  and  $L_1$  and 30 steps for elastic. Single adversarial training baselines are also shown.

Training parameters (ResNet-50)	$L_\infty$ train	other train	$L_\infty$ val	other val
$L_\infty \varepsilon = 8$ , Elastic $\varepsilon = 4$ , Seed 1	90	89	35	74
$L_\infty \varepsilon = 8$ , Elastic $\varepsilon = 4$ , Seed 2	89	90	47	44
$L_\infty \varepsilon = 16$ , $L_1 \varepsilon = 612000$ , Seed 1	86	87	22	16
$L_\infty \varepsilon = 16$ , $L_1 \varepsilon = 612000$ , Seed 2	88	87	16	24
$L_\infty \varepsilon = 8$	81	–	74	–
$L_\infty \varepsilon = 16$	68	–	63	–
Elastic $\varepsilon = 4$	–	88	–	76
$L_1 \varepsilon = 612000$	–	75	–	59

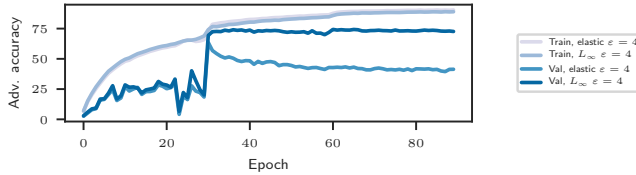


Figure 6: Train and validation curves for joint training against  $L_\infty$ ,  $\varepsilon = 4$  and Elastic,  $\varepsilon = 4$ . The validation accuracy of Elastic decreases as training progresses, indicating overfitting.

likely. We briefly investigate the relation between overfitting and model capacity in Appendix E.2; validation accuracy appears to increase slightly when using a ResNet-101, but overfitting remains.

## 5 Comparing unforeseen adversarial distortions and common corruptions

“Common” visual corruptions such as (non-adversarial) fog, blur, or pixelation have emerged as another avenue for measuring the robustness of computer vision models [26, 12, 27]. Recent work [11] suggests that robustness to such common corruptions is linked to adversarial robustness and proposes corruption robustness as an easily computed indicator of adversarial robustness. We consider this as an alternative to our methodology by testing the corruption robustness of our adversarially trained models on the ImageNet-C benchmark.

**Experimental setup and results.** We evaluate our adversarially trained models on the 100-class subset of the corruption robustness benchmark ImageNet-C introduced in [12], using the same classes as ImageNet-100. We call this subset ImageNet-C-100; it consists of the ImageNet-100 validation set with 19 common corruptions applied at 5 levels of severity. We use the JPEG files available at <https://github.com/hendrycks/robustness>. Figure 7 reports average accuracies by distortion type.

**Adversarial training against small distortions increases corruption robustness.** The first column of each block in Figure 7 shows that training against small adversarial distortions generally increases average accuracy compared to an undefended model. However, training against larger distortions often decreases average accuracy, largely due to the resulting decrease in clean accuracy.

**Adversarial distortions and common corruptions can affect defenses differently.** Our  $L_p$ -JPEG and elastic attacks are adversarial versions of the corresponding common corruptions. While training against adversarial JPEG at larger  $\varepsilon$  improves robustness against adversarial JPEG attacks (Figure 9 in Appendix C.1), Figure 7 shows that robustness against common JPEG corruptions decreases as we adversarially train against JPEG at larger  $\varepsilon$ , though it remains better than for normally trained models. Similarly, adversarial Elastic training at large  $\varepsilon$  begins to hurt robustness to its common counterpart. This is likely because common corruptions are easier than adversarial distortions, hence the increased robustness does not make up for the decreased clean accuracy.

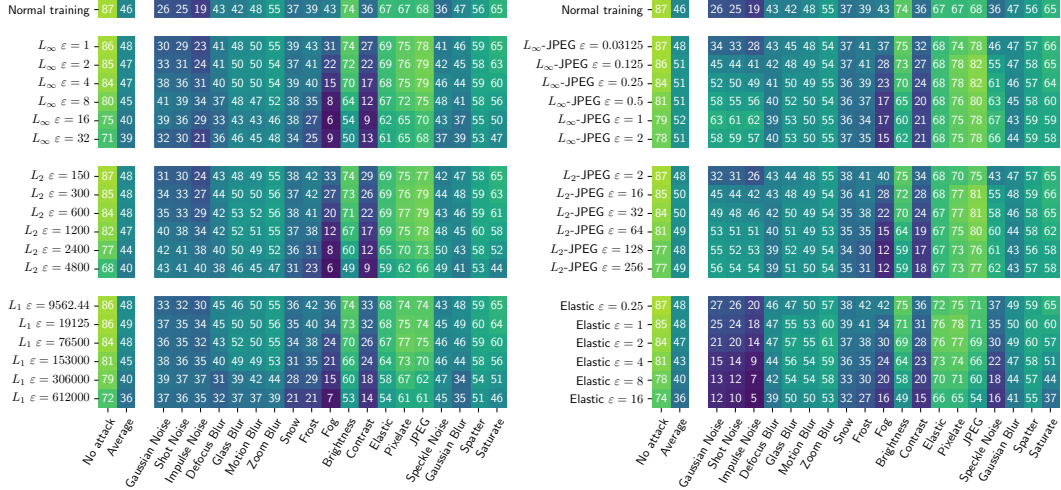


Figure 7: Accuracies of defenses (rows) on ImageNet-C-100 corruptions (columns).

## 6 Discussion and Related Work

We have seen that robustness against one attack provides limited information about robustness to other attacks, and moreover that adversarial training provides limited robustness against unforeseen attacks. These results suggest a need to modify or move beyond adversarial training. While joint adversarial training is one possible alternative, we have seen that it often leads to overfitting. Even ignoring this, it is not clear that joint training would confer robustness to attacks that are different from both of the training attacks.

Evaluating robustness has proven difficult, necessitating detailed study of best practices even for a single fixed attack [28, 29]. We build on these best practices by showing how to choose and calibrate a diverse set of unforeseen attacks. Our work is a supplement to existing practices, not a replacement—we strongly recommend following the guidelines in [28] and [29] in addition to our recommendations.

Some caution is necessary when interpreting specific numeric results in our paper. Many previous implementations of adversarial training fell prone to gradient masking [28, 30], with apparently successful training occurring only recently [3, 4]. While evaluating with moderately many PGD steps (200) helps guard against this, [31] shows that an  $L_\infty$ -trained model that appeared robust against  $L_2$  actually had substantially less robustness when evaluating with  $10^6$  PGD steps. If this effect is pervasive, then there may be even less transfer between attacks than our current results suggest.

For evaluating against a fixed attack, DeepFool [32] and CLEVER [33] can be seen as existing alternatives to our calibration methodology, which roughly work by computing the expected minimum  $\epsilon$  to successfully attack an image. However, these methods apply only to attacks which optimize over an  $L_p$ -ball of radius  $\epsilon$ , and CLEVER can be susceptible to gradient masking [34].

Our results add to a growing line of evidence that evaluating against a single known attack type provides a misleading picture of the robustness of a model [35, 5, 9, 10, 8]. Going one step further, we believe that robustness itself provides only a narrow window into a model’s behavior; in addition to robustness, we should seek to build a diverse toolbox for understanding machine learning models, including visualization [36, 37], disentanglement of relevant features [27], and measuring extrapolation to different datasets [38] or to the long tail of natural but unusual inputs [39]. Together, these windows into model behavior can give us a clearer picture of how to make models reliable in the real world.

## Acknowledgements

D. K., Y. S., and J. S. were supported by a grant from the Open Philanthropy Project. D. K. was supported by NSF Grant DGE-1656518. Y. S. was supported by a Junior Fellow award from the

Simons Foundation and NSF Grant DMS-1701654. D. H. was supported by NSF Frontier Award 1804794. Work by D. K. and Y. S. was partially done at OpenAI.

## References

- [1] Kaiming He, Xiangyu Zhang, Shaoqing Ren, and Jian Sun. Identity mappings in deep residual networks. In *European conference on computer vision*, pages 630–645. Springer, 2016.
- [2] Ian J Goodfellow, Jonathon Shlens, and Christian Szegedy. Explaining and harnessing adversarial examples. *arXiv preprint arXiv:1412.6572*, 2014.
- [3] Aleksander Madry, Aleksandar Makelov, Ludwig Schmidt, Dimitris Tsipras, and Adrian Vladu. Towards deep learning models resistant to adversarial attacks. *arXiv preprint arXiv:1706.06083*, 2017.
- [4] Cihang Xie, Yuxin Wu, Laurens van der Maaten, Alan Yuille, and Kaiming He. Feature denoising for improving adversarial robustness. *arXiv preprint arXiv:1812.03411*, 2018.
- [5] Logan Engstrom, Brandon Tran, Dimitris Tsipras, Ludwig Schmidt, and Aleksander Madry. A rotation and a translation suffice: Fooling CNNs with simple transformations. *arXiv preprint arXiv:1712.02779*, 2017.
- [6] Tom B. Brown, Dandelion Mané, Aurko Roy, Martín Abadi, and Justin Gilmer. Adversarial patch. *CoRR*, abs/1712.09665, 2017.
- [7] Anish Athalye, Logan Engstrom, Andrew Ilyas, and Kevin Kwok. Synthesizing robust adversarial examples. *CoRR*, abs/1707.07397, 2017.
- [8] Jörn-Henrik Jacobsen, Jens Behrmann, Nicholas Carlini, Florian Tramèr, and Nicolas Papernot. Exploiting excessive invariance caused by norm-bounded adversarial robustness, 2019.
- [9] Matt Jordan, Naren Manoj, Surbhi Goel, and Alexandros G. Dimakis. Quantifying Perceptual Distortion of Adversarial Examples. *arXiv e-prints*, page arXiv:1902.08265, Feb 2019.
- [10] Florian Tramèr and Dan Boneh. Adversarial Training and Robustness for Multiple Perturbations. *arXiv e-prints*, page arXiv:1904.13000, Apr 2019.
- [11] Nic Ford, Justin Gilmer, Nicolas Carlini, and Dogus Cubuk. Adversarial examples are a natural consequence of test error in noise. *arXiv preprint arXiv:1901.10513*, 2019.
- [12] Dan Hendrycks and Thomas Dietterich. Benchmarking neural network robustness to common corruptions and perturbations. In *International Conference on Learning Representations*, 2019.
- [13] Christian Szegedy, Wojciech Zaremba, Ilya Sutskever, Joan Bruna, Dumitru Erhan, Ian Goodfellow, and Rob Fergus. Intriguing properties of neural networks. *arXiv preprint arXiv:1312.6199*, 2013.
- [14] Nicholas Carlini and David Wagner. Towards evaluating the robustness of neural networks. In *2017 IEEE Symposium on Security and Privacy (SP)*, pages 39–57. IEEE, 2017.
- [15] Pin-Yu Chen, Yash Sharma, Huan Zhang, Jinfeng Yi, and Cho-Jui Hsieh. EAD: Elastic-net attacks to deep neural networks via adversarial examples. In *Thirty-second AAAI conference on artificial intelligence*, 2018.
- [16] Chaowei Xiao, Jun-Yan Zhu, Bo Li, Warren He, Mingyan Liu, and Dawn Song. Spatially transformed adversarial examples. *arXiv preprint arXiv:1801.02612*, 2018.
- [17] Richard Shin and Dawn Song. JPEG-resistant adversarial images. In *NIPS 2017 Workshop on Machine Learning and Computer Security*, 2017.
- [18] Ares Lagae, Sylvain Lefebvre, George Drettakis, and Philip Dutré. Procedural noise using sparse gabor convolution. *ACM Trans. Graph.*, 28(3):54:1–54:10, July 2009.
- [19] Kenneth T. Co, Luis Muñoz-González, and Emil C. Lupu. Sensitivity of deep convolutional networks to gabor noise. *CoRR*, abs/1906.03455, 2019.

- [20] Dan Hendrycks and Thomas G Dietterich. Benchmarking neural network robustness to common corruptions and surface variations. *arXiv preprint arXiv:1807.01697*, 2018.
- [21] Marguerite Frank and Philip Wolfe. An algorithm for quadratic programming. *Naval research logistics quarterly*, 3(1-2):95–110, 1956.
- [22] Jia Deng, Wei Dong, Richard Socher, Li-Jia Li, Kai Li, and Li Fei-Fei. Imagenet: A large-scale hierarchical image database. In *2009 IEEE conference on computer vision and pattern recognition*, pages 248–255. IEEE, 2009.
- [23] Arkadi Nemirovski and D Yudin. On Cezari’s convergence of the steepest descent method for approximating saddle point of convex-concave functions. In *Soviet Math. Dokl*, volume 19, pages 258–269, 1978.
- [24] Arkadi Nemirovski and D Yudin. *Problem Complexity and Method Efficiency in Optimization*. Intersci. Ser. Discrete Math. Wiley, New York, 1983.
- [25] Nicholas Carlini, Anish Athalye, Nicolas Papernot, Wieland Brendel, Jonas Rauber, Dimitris Tsipras, Ian J. Goodfellow, Aleksander Madry, and Alexey Kurakin. On evaluating adversarial robustness. *CoRR*, abs/1902.06705, 2019.
- [26] Igor Vasiljevic, Ayan Chakrabarti, and Gregory Shakhnarovich. Examining the impact of blur on recognition by convolutional networks. *CoRR*, abs/1611.05760, 2016.
- [27] Robert Geirhos, Patricia Rubisch, Claudio Michaelis, Matthias Bethge, Felix A. Wichmann, and Wieland Brendel. Imagenet-trained cnns are biased towards texture; increasing shape bias improves accuracy and robustness. *CoRR*, abs/1811.12231, 2018.
- [28] Nicolas Papernot, Patrick McDaniel, Ian Goodfellow, Somesh Jha, Z Berkay Celik, and Ananthram Swami. Practical black-box attacks against machine learning. In *Proceedings of the 2017 ACM on Asia conference on computer and communications security*, pages 506–519. ACM, 2017.
- [29] Anish Athalye, Nicholas Carlini, and David Wagner. Obfuscated gradients give a false sense of security: Circumventing defenses to adversarial examples. *arXiv preprint arXiv:1802.00420*, 2018.
- [30] Logan Engstrom, Andrew Ilyas, and Anish Athalye. Evaluating and understanding the robustness of adversarial logit pairing. *arXiv preprint arXiv:1807.10272*, 2018.
- [31] Haifeng Qian and Mark N. Wegman. L2-nonexpansive neural networks. In *International Conference on Learning Representations (ICLR)*, 2019.
- [32] Seyed-Mohsen Moosavi-Dezfooli, Alhussein Fawzi, and Pascal Frossard. Deepfool: a simple and accurate method to fool deep neural networks. corr abs/1511.04599 (2015). *arXiv preprint arXiv:1511.04599*, 2015.
- [33] Tsui-Wei Weng, Huan Zhang, Pin-Yu Chen, Jinfeng Yi, Dong Su, Yupeng Gao, Cho-Jui Hsieh, and Luca Daniel. Evaluating the robustness of neural networks: An extreme value theory approach. *arXiv preprint arXiv:1801.10578*, 2018.
- [34] Ian Goodfellow. Gradient masking causes clever to overestimate adversarial perturbation size. *arXiv preprint arXiv:1804.07870*, 2018.
- [35] Yash Sharma and Pin-Yu Chen. Attacking the Madry Defense Model with  $L_1$ -based Adversarial Examples. *arXiv e-prints*, page arXiv:1710.10733, Oct 2017.
- [36] Chris Olah, Arvind Satyanarayan, Ian Johnson, Shan Carter, Ludwig Schubert, Katherine Ye, and Alexander Mordvintsev. The building blocks of interpretability. *Distill*, 2018. <https://distill.pub/2018/building-blocks>.
- [37] Tianyuan Zhang and Zhanxing Zhu. Interpreting adversarially trained convolutional neural networks. In *International Conference on Machine Learning (ICML)*, 2019.

- [38] Antonio Torralba and Alexei A. Efros. Unbiased look at dataset bias. In *IEEE Conference on Computer Vision and Pattern Recognition (CVPR)*, 2011.
- [39] Dan Hendrycks, Kevin Zhao, Steven Basart, Jacob Steinhardt, and Dawn Song. Natural adversarial examples. *arXiv preprint arXiv:1907.07174*, 2019.
- [40] Priya Goyal, Piotr Dollár, Ross Girshick, Pieter Noordhuis, Lukasz Wesolowski, Aapo Kyrola, Andrew Tulloch, Yangqing Jia, and Kaiming He. Accurate, large minibatch SGD: Training Imagenet in 1 hour. *arXiv preprint arXiv:1706.02677*, 2017.

## A Training hyperparameters

For ImageNet-100, we trained on machines with 8 NVIDIA V100 GPUs using standard data augmentation [1]. Following best practices for multi-GPU training [40], we ran synchronized SGD for 90 epochs with batch size  $32 \times 8$  and a learning rate schedule with 5 “warm-up” epochs and a decay at epochs 30, 60, and 80 by a factor of 10. Initial learning rate after warm-up was 0.1, momentum was 0.9, and weight decay was  $10^{-4}$ . For CIFAR-10, we trained on a single NVIDIA V100 GPU for 200 epochs with batch size 32, initial learning rate 0.1, momentum 0.9, and weight decay  $10^{-4}$ . We decayed the learning rate at epochs 100 and 150.

---

**Algorithm 1** Pseudocode for the Frank-Wolfe algorithm for the  $L_1$  attack.

---

```

1: Input: function  $f$ , initial input  $x \in [0, 1]^d$ ,  $L_1$  radius  $\rho$ , number of steps  $T$ .
2: Output: approximate maximizer  $\bar{x}$  of  $f$  over the truncated  $L_1$  ball  $B_1(\rho; x) \cap [0, 1]^d$  centered at  $x$ .
3:
4:  $x^{(0)} \leftarrow \text{RandomInit}(x)$  ▷ Random initialization
5: for  $t = 1, \dots, T$  do
6:    $g \leftarrow \nabla f(x^{(t-1)})$  ▷ Obtain gradient
7:   for  $k = 1, \dots, d$  do
8:      $s_k \leftarrow$  index of the coordinate of  $g$  by with  $k^{\text{th}}$  largest norm
9:   end for
10:   $S_k \leftarrow \{s_1, \dots, s_k\}$ .
11:
12:  for  $i = 1, \dots, d$  do ▷ Compute move to boundary of  $[0, 1]$  for each coordinate.
13:    if  $g_i > 0$  then
14:       $b_i \leftarrow 1 - x_i$ 
15:    else
16:       $b_i \leftarrow -x_i$ 
17:    end if
18:  end for
19:   $M_k \leftarrow \sum_{i \in S_k} |b_i|$  ▷ Compute  $L_1$ -perturbation of moving  $k$  largest coordinates.
20:   $k^* \leftarrow \max\{k \mid M_k \leq \rho\}$  ▷ Choose largest  $k$  satisfying  $L_1$  constraint.
21:  for  $i = 1, \dots, d$  do ▷ Compute  $\hat{x}$  maximizing  $g^\top x$  over the  $L_1$  ball.
22:    if  $i \in S_{k^*}$  then
23:       $\hat{x}_i \leftarrow x_i + b_i$ 
24:    else if  $i = s_{k^*+1}$  then
25:       $\hat{x}_i \leftarrow x_i + (\rho - M_{k^*}) \text{sign}(g_i)$ 
26:    else
27:       $\hat{x}_i \leftarrow x_i$ 
28:    end if
29:  end for
30:   $x^{(t)} \leftarrow (1 - \frac{1}{t})x^{(t-1)} + \frac{1}{t}\hat{x}$  ▷ Average  $\hat{x}$  with previous iterates
31: end for
32:  $\bar{x} \leftarrow x^{(T)}$ 

```

---

## B $L_1$ Attack

We chose to use the Frank-Wolfe algorithm for optimizing the  $L_1$  attack, as Projected Gradient Descent would require projecting onto a truncated  $L_1$  ball, which is a complicated operation. In contrast, Frank-Wolfe only requires optimizing linear functions  $g^\top x$  over a truncated  $L_1$  ball; this can be done by sorting coordinates by the magnitude of  $g$  and moving the top  $k$  coordinates to the boundary of their range (with  $k$  chosen by binary search). This is detailed in Algorithm 1.



## C Full evaluation results

### C.1 Full evaluation results and analysis for ImageNet-100

We show the full results of all adversarial attacks against all adversarial defenses for ImageNet-100 in Figure 8. As described, the  $L_p$  attacks and defenses give highly correlated information on held-out defenses and attacks respectively. Thus, we recommend evaluating on a wide range of distortion types. Full UAR scores are also provided for ImageNet-100 in Figure 9.

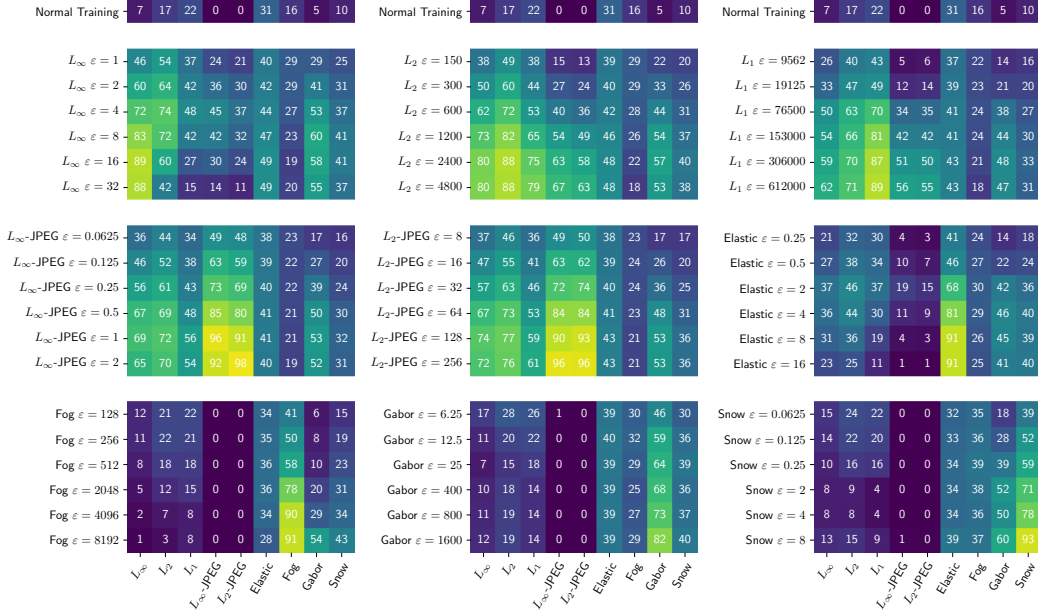


Figure 9: UAR scores (multiplied by 100) for adv. trained defenses (rows) against distortion types (columns) for ImageNet-100.

We further show selected results in Figure 10. As shown, a wide range of  $\epsilon$  is required to see the full behavior.

### C.2 $L_1$ -JPEG and $L_2$ -JPEG

We compare the  $L_1$ -JPEG and  $L_2$ -JPEG attacks in Figure 11. As shown, the attacks are similar. As such, we omit  $L_1$ -JPEG in the full analysis for brevity and visibility.

### C.3 Full evaluation results and analysis for CIFAR-10

#### C.3.1 Full results for CIFAR10

We show the results of adversarial attacks and defenses for CIFAR-10 in Figure 12. We experienced difficulty training the  $L_2$  and  $L_1$  attacks at distortion sizes greater than those shown and have omitted those runs, which we believe may be related to the small size of CIFAR-10 images.

#### C.3.2 ATA and UAR for CIFAR-10

The  $\epsilon$  calibration procedure for CIFAR-10 was similar to that used for ImageNet-100. We started with the perceptually small  $\epsilon_{\min}$  values in Table 3 and increased  $\epsilon$  geometrically with ratio 2 until adversarial accuracy of an adversarially trained model dropped below 40. Note that this threshold is higher for CIFAR-10 because there are fewer classes. The resulting ATA and UAR values for CIFAR10 are shown in Table 3 and Figure 13. We omitted calibration for the  $L_2$ -JPEG attack because we chose too small a range of  $\epsilon$  for our initial training experiments, and we plan to address this issue in the future.

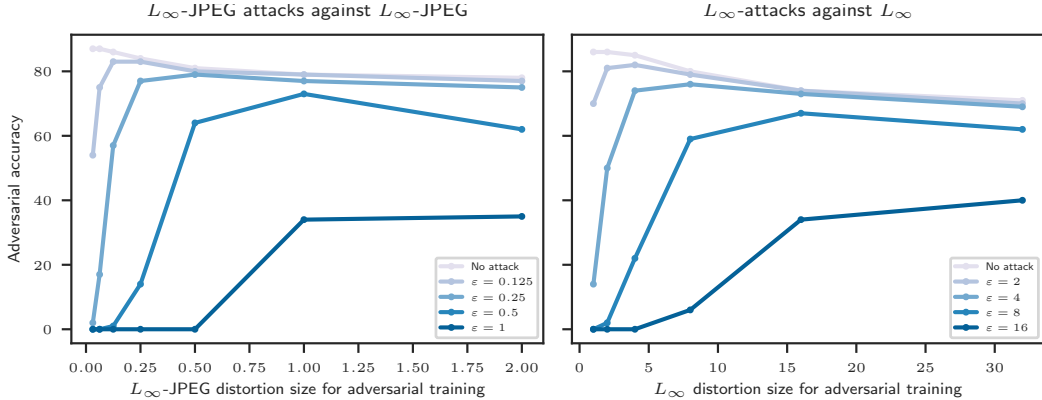


Figure 10: Adversarial accuracies of attacks on adversarially trained models for different distortion sizes on ImageNet-100. For a given attack  $\varepsilon$ , the best  $\varepsilon'$  to train against satisfies  $\varepsilon' > \varepsilon$  because the random scaling of  $\varepsilon'$  during adversarial training ensures that a typical distortion during adversarial training has size smaller than  $\varepsilon'$ .

Table 3: Calibrated distortion sizes and ATA values for ResNet-56 on CIFAR-10

Attack	$\varepsilon_1$	$\varepsilon_2$	$\varepsilon_3$	$\varepsilon_4$	$\varepsilon_5$	$\varepsilon_6$	ATA <sub>1</sub>	ATA <sub>2</sub>	ATA <sub>3</sub>	ATA <sub>4</sub>	ATA <sub>5</sub>	ATA <sub>6</sub>
$L_\infty$	1	2	4	8	16	32	91.0	87.8	81.6	71.3	46.5	23.1
$L_2$	40	80	160	320	640	2560	90.1	86.4	79.6	67.3	49.9	17.3
$L_1$	195	390	780	1560	6240	24960	92.2	90.0	83.2	73.8	47.4	35.3
$L_\infty$ -JPEG	0.03125	0.0625	0.125	0.25	0.5	1	89.7	87.0	83.1	78.6	69.7	35.4
$L_1$ -JPEG	2	8	64	256	512	1024	91.4	88.1	80.2	68.9	56.3	37.7
Elastic	0.125	0.25	0.5	1	2	8	87.4	81.3	72.1	58.2	45.4	27.8

## D Robustness of our results

### D.1 Replication

We replicated our results for the first three rows of Figure 8 with different random seeds to see the variation in our results. As shown in Figure 14, deviations in results are minor.

### D.2 Convergence

We replicated the results in Figure 8 with 50 instead of 200 steps to see how the results changed based on the number of steps in the attack. As shown in Figure 15, the deviations are minor.

## E Further Results for Joint Training

### E.1 Full experimental results

We show the evaluation accuracies of jointly trained models in Figure 16.

We show all the attacks against the jointly adversarially trained defenses in Figure 17.

### E.2 Overfitting and model capacity

As a first test to understand the relationship between model capacity and overfitting, we trained ResNet-101 models using the same procedure as in Section 4.3. Briefly, overfitting still occurs, but ResNet-101 achieves a few percentage points higher than ResNet-50.

We show the training curves in Figure 18 and the training and validation numbers in Table 4.

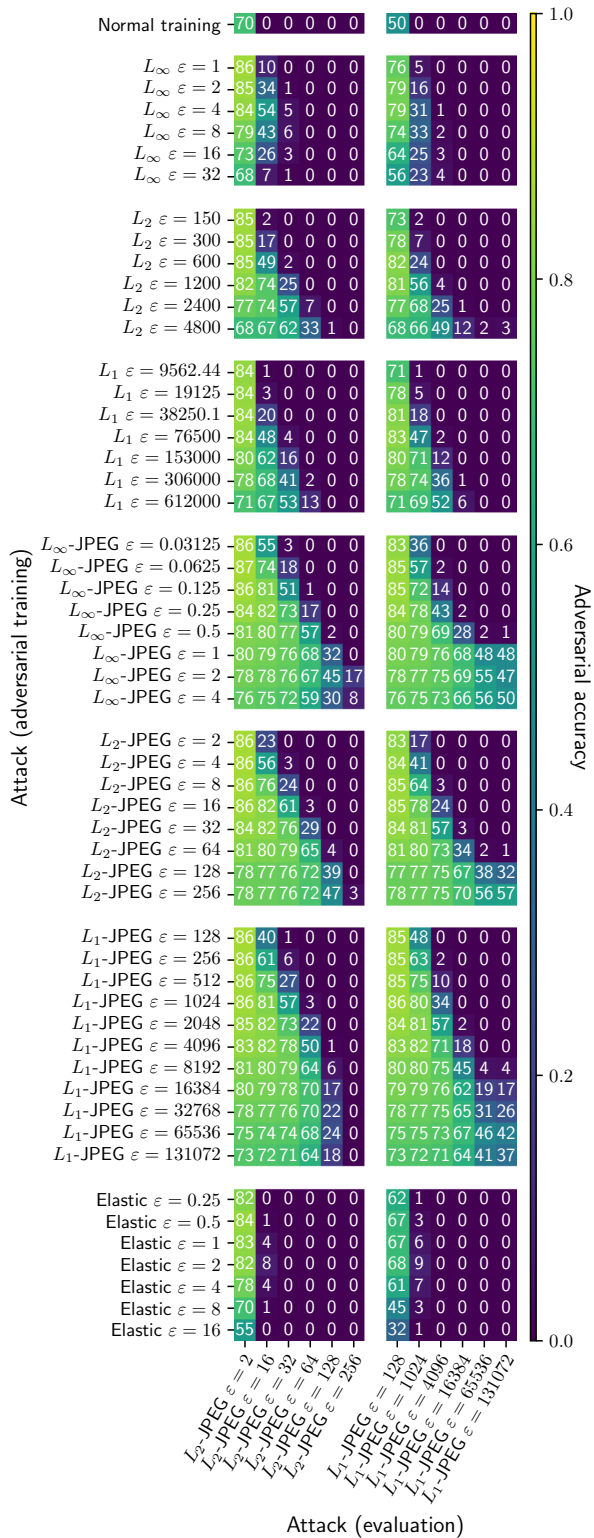


Figure 11: A comparison of  $L_1$ -JPEG and  $L_2$ -JPEG attacks.

## F Further discussion of corruption robustness

We collect here a few more implications regarding robustness transfer to common corruptions.

Table 4: Training and validation numbers for ResNet-101 and ResNet-50 for joint training against  $L_\infty$ ,  $\varepsilon = 8$  and elastic,  $\varepsilon = 4$ .

Training parameters	$L_\infty$ train	other train	$L_\infty$ val	other val
$L_\infty \varepsilon = 8$ , Elastic $\varepsilon = 4$ , ResNet-50 Seed 1	90	89	35	74
$L_\infty \varepsilon = 8$ , Elastic $\varepsilon = 4$ , ResNet-50 Seed 2	89	90	47	44
$L_\infty \varepsilon = 8$ , Elastic $\varepsilon = 4$ ResNet-101	90	91	49	46

**Training against  $L_p$ -JPEG is more robust than training against  $L_p$  on noise.** Figure 7 reveals that training against  $L_p$ -JPEG is more effective than training against  $L_p$  for the noise distortions in the first three columns. On the other hand, training against elastic *hurts* performance on noise.

**Adversarial training is not robust against fog, brightness, and contrast.** Figure 7 shows that almost every adversarially trained model performs worse on these distortions than an undefended model, which agrees with an observation of [11] for fog and contrast on CIFAR-10-C. This is especially surprising because brightness and contrast are distortions with only one free parameter.



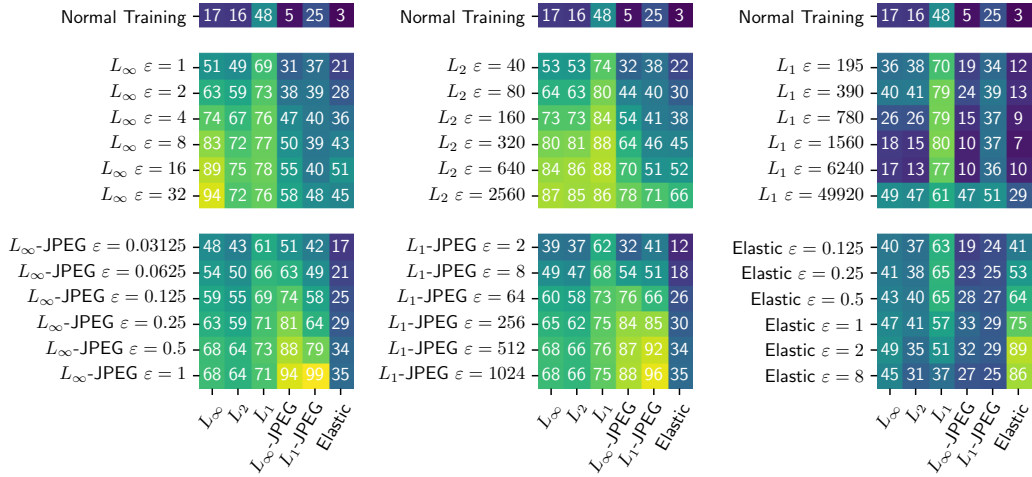


Figure 13: UAR scores on CIFAR-10. Displayed UAR scores are multiplied by 100 for clarity.

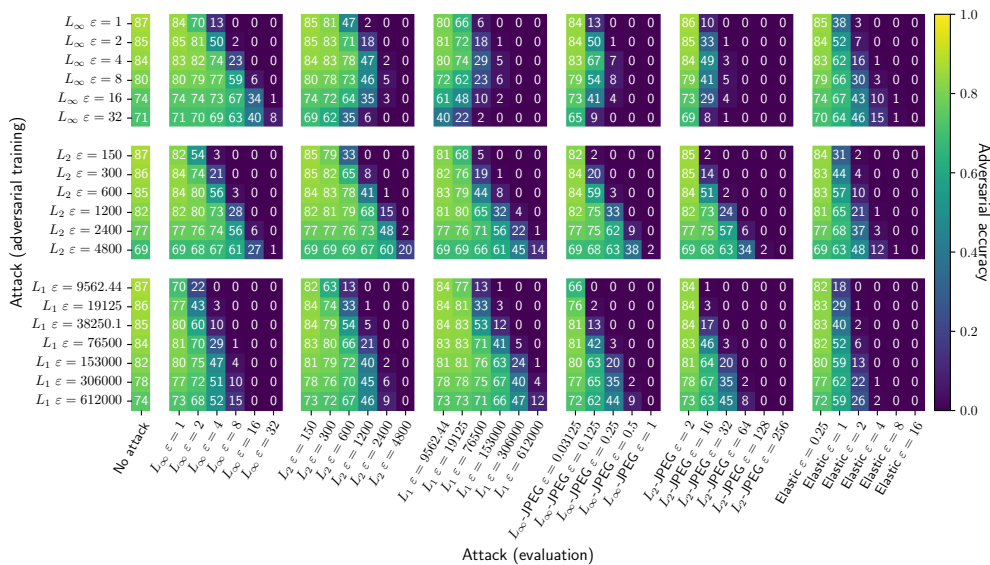


Figure 14: Replica of the first three block rows of Figure 8 with different random seeds. Deviations in results are minor.

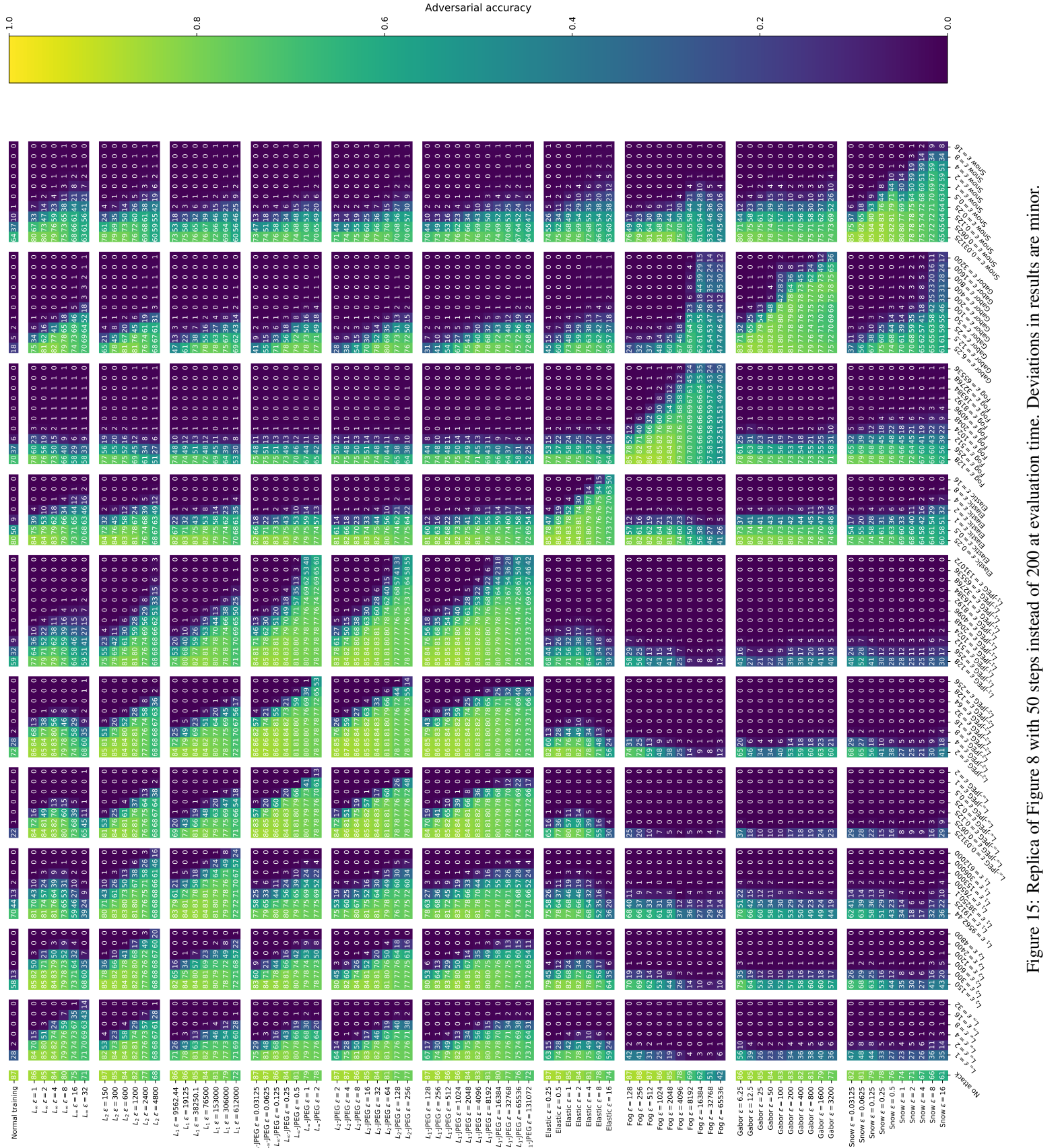


Figure 15: Replica of Figure 8 with 50 steps instead of 200 at evaluation time. Deviations in results are minor.

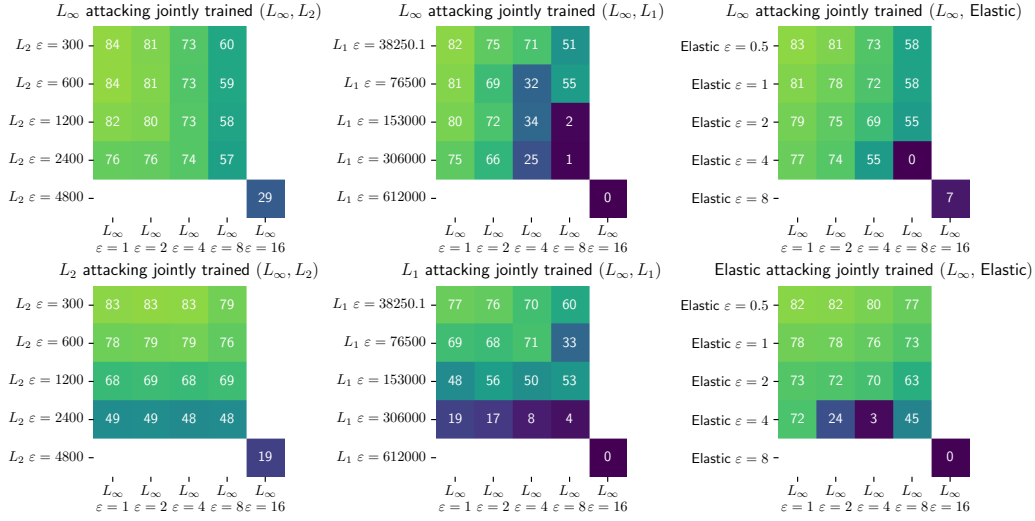


Figure 16: Evaluation accuracies of jointly trained models. Attack and training  $\epsilon$  values are equal.

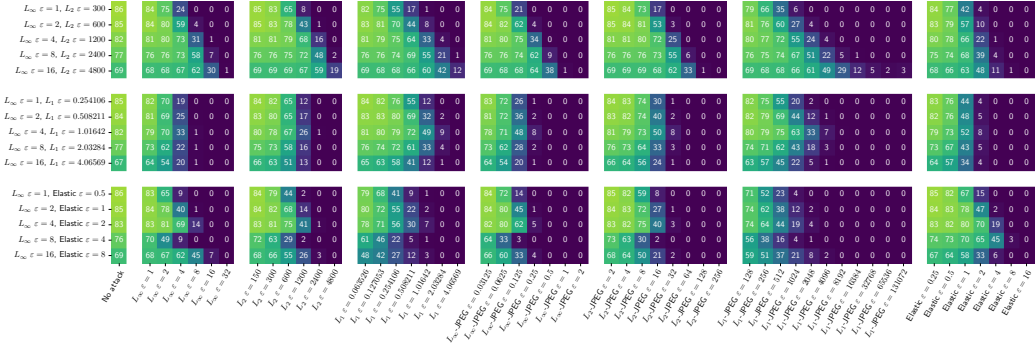


Figure 17: All attacks (columns) vs. jointly adversarially trained defense (rows).

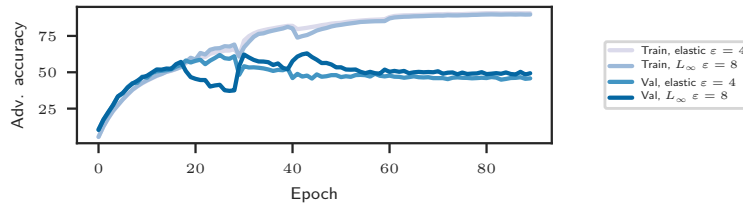


Figure 18: Train and validation curves for joint training against  $L_\infty$ ,  $\epsilon = 4$  and elastic,  $\epsilon = 8$  using ResNet-101. As shown, the validation accuracies decrease as training progresses, indicating overfitting.